Facile Preparation of Organic Nanoparticles by Interfacial Cross-Linking of Reverse Micelles and Template Synthesis of Subnanometer Au–Pt Nanoparticles

Shiyong Zhang and Yan Zhao*

Department of Chemistry, Iowa State University, Ames, Iowa 50011-3111, United States

ABSTRACT A single- and a double-tailed cationic surfactant with the triallylammonium headgroup formed reverse micelles (RMs) in heptane/chloroform containing a small amount of water. The reverse micelles were cross-linked at the interface upon UV irradiation in the presence of a water-soluble dithiol cross-linker and a photoinitiator. The resulting interfacially cross-linked reverse micelles (ICRMs) of the single-tailed surfactant aggregated in a solvent-dependent fashion, whereas those of the double-tailed were identical in size as the corresponding RMs. The ICRMs could extract anionic metal salts, such as $AuCl_4^-$ and $PtCl_6^{2-}$, from water into the organic phase. Au and Pt metal nanoparticles were produced upon reduction of metal salts. The covalent nature of the ICRMs made the template synthesis highly predictable, with the size of the metal particles controlled by the amount of the metal salt and the method of reduction. Nanoalloys were obtained by combining two metal precursors in the same reaction. Reduction of the ICRM-entrapped aurate also occurred without any external reducing agents, and the gold nanoparticles differed dramatically from those obtained through sodium borohydride reduction. The same template allowed the preparation of luminescent Au_4, Au_8, and Au_{13}–Au_{23} clusters, as well as gold nanoparticles several nanometers in size, simply by using different amounts of gold precursor and reducing conditions.

KEYWORDS: template synthesis · reverse micelle · thiol–ene reaction · gold clusters · nanoalloy · luminescence

Surfactants can self-assemble into a rich array of ordered phases depending on their molecular structure, temperature, and the amounts of polar, nonpolar, and surfactant ingredients present. There has been a long-standing interest in capturing these phases by covalent bonds to prepare ordered nanomaterials.[1–5] Covalent capture of micelles,[6–9] vesicles,[10–14] inverted hexagonal phases,[15–18] and even bicontinuous phases[19–22] of small-molecule amphiphiles has all met with considerable success and been thoroughly reviewed.[1–5] Fixing these self-assembled phases with covalent bonds not only enhances their stability but also enables their practical applications including as templates for further material synthesis. Gin and co-workers, for example, employed cross-linked liquid crystalline phases of surfactants for nanocomposite preparation,[23] size-selective filtration,[24] catalysis,[25] and lithium conduction.[19]

Reverse micelles (RMs) are formed when a small amount of water is added to a mixture of a suitable surfactant in nonpolar solvent(s). RMs are widely utilized as media for catalysis and templates to prepare inorganic nanomaterials.[26,27] Nevertheless, the dimension of the inorganic materials obtained from the template synthesis rarely correlates directly with the size of the RM templates. Collision of these dynamic, noncovalent assemblies results in coalescence as well as rapid exchange of the entrapped water and dissolved contents, making it difficult to predict the size and morphology of the final materials.[28,29]

Covalent capture of the RMs is expected to circumvent these problems. Once the RMs are fixed by covalent bonds, intermicellar exchange of water can only happen if water molecules leave the core of one cross-linked RM, enter the nonpolar solvents, and get into the core of another cross-linked RM. The energetic cost associated with such a process is unthinkable. In addition, a cross-linked RM has well-defined boundary, unlike the parent RM. Growth of inorganic materials within a RM template thus will be confined within the hydrophilic core, and the size of the inorganic nanoparticles should be controlled directly by the amount of the metal precursors used in the synthesis.

Unfortunately, the same problems plaguing the RM-templated synthesis also plague its covalent capture. The exchange of

* Address correspondence to zhaoy@iastate.edu.

Received for review October 6, 2010 and accepted March 2, 2011.

Published online March 02, 2011
10.1021/nn102666k

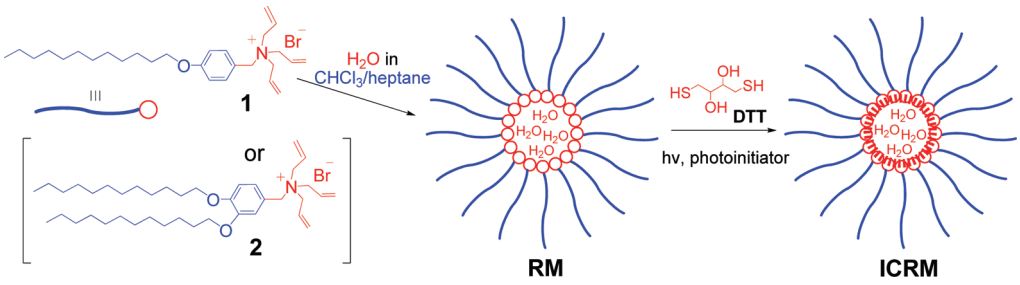

Scheme 1. Preparation of ICRMs by the thiol−ene addition.

surfactants between different RMs *via* intermicellar collision is nearly diffusion-controlled, far exceeding the rate of most chemical reactions including free radical polymerization. For this reason, free radical polymerization of surfmers (*i.e.*, polymerizable surfactants) is not confined within a single reverse micelle.[30] Before a growing polymer radical reacts with another monomer, it has experienced many intermicellar collision, coalescence, and division. This was probably why, when De Schryver *et al.* polymerized *N*,*N*-didodecyl-*N*-methyl-*N*-(2-(methacryloyloxy)ethyl) ammonium in the RM configuration, they obtained polymers with molecular weights significantly higher than those of the original RMs.[31] For many years, cross-linking of RMs received little attention while cross-linking of other surfactant phases was studied intensively.[1−5] It was not until recently that McQuade and co-workers reported the first example to capture RMs by free radical polymerization and obtained spherical particles ~7−12 nm in diameter.[32,33] The key to success was the design of an AOT-like surfactant with two polymerizable groups in the midsection of the molecule.

In this paper, we employ the highly efficient thiol−ene "click" reaction[34−36] to cross-link RMs exclusively at the interface. The interfacially cross-linked reverse micelles (ICRMs) were found to have highly unusual properties as templates for metal nanoparticle synthesis. Different reducing conditions had an enormous impact on the nanoparticle production. Nanoalloys were simply obtained by combining two metal precursors in the same reaction. Noble metal clusters recently have shown great promise in their applications in photonics[37−47] and catalysis.[48−52] In the literature, subnanometer gold clusters were usually prepared with dendrimers templates, which require multiple steps for synthesis. The reaction was reported to take days to complete, and postpurification (*e.g.*, centrifugation) was needed to remove large particles formed as side products.[38,40] In contrast, the synthesis of both the cross-linkable surfactant and the ICRMs was extremely simple in our method. The template synthesis was also fast and straightforward to control.

RESULTS AND DISCUSSION

Design, Synthesis, and Cross-Linking of Surfactants in the RM Configuration. Both the structure of the cross-linkable surfactant and the cross-linking reaction are critical to the covalent capture of RMs. Because the stability of a RM mainly derives from the noncovalent interactions at the core, the cross-linkable groups should be near the headgroup of the surfactant. As the cross-linkable groups move away from the headgroup (toward and along the hydrophobic tail), the cross-linked RM will become more dependent upon noncovalent interactions for core stabilization and the likelihood of intermicellar cross-linking will increase in the meantime. Another important requirement for the system is that the cross-linking reaction should cause minimal disturbance to the packing of the surfactants in the RM, or the structure would reconfigure itself during cross-linking. High cross-linking density, especially near the core, is beneficial by maximizing the stability of the cross-linked RM. A fast cross-linking reaction is also desirable, potentially allowing the structure to be set before any reconfiguration can take place.

Although it is possible to prepare cross-linked RMs with free radical polymerization,[32] we reasoned that another reaction, the so-called thiol−ene reaction,[34−36] has several attractive features for the purpose. First, the reaction is extremely efficient, even in highly demanding situations such as the synthesis of dendrimers[53,54] and selective functionalization of proteins.[55] Second, incorporation of vinyl (*i.e.*, ene) groups is extremely simple in a surfactant. Cationic surfactant **1** (Scheme 1), for example, contained three vinyl groups in the headgroup and can be prepared easily from commercially available materials. Having three cross-linkable groups in a concentrated fashion enhances the cross-linking density at the core and is advantageous to the stability of the cross-linked micelle. Third, there is great flexibility in the structure of thiol cross-linkers. In particular, if the distance between the thiol groups matches reasonably well with the average distance between the surfactant headgroups in the RM, cross-linking should cause minimal disturbance to the packing of the surfactants. Free radical polymerization of vinyl monomers, on the other hand, tends to make the structure more compact. Fourth, the thiol−ene reaction has excellent tolerance for functional groups.[34−36] A wide range of commercially available thiol cross-linkers may be used, and introduction of additional functional groups to the RM is straightforward.

Surfactant **1** was prepared by alkylation of 4-hydroxybenzaldehyde with 1-bromododecane, reduction of the aldehyde with sodium borohydride, bromination of the resulting alcohol with phosphorus tribromide, and nucleophilic displacement of the bromide with triallyl amine. Optically clear RM solutions were obtained in a 2:1 heptane/chloroform mixture with W_0 up to 15 (W_0 = [H_2O]/[**1**]). Similar conditions were reported to allow single-tailed CTAB (hexadecyltrimethylammonium bromide) to form RMs.[56] Although RMs could form without chloroform in our hands, this solvent was needed to dissolve the cross-linker (dithiothreitol or DTT) in the nonpolar solvent mixture. We chose DTT as the cross-linker with the hypothesis that the water pool inside the RM would dissolve some of the hydrophilic dithiol. In this way, the vinyl and thiol reactive groups are brought into close proximity, which would greatly accelerate the already fast free radical chain reaction. A double-tailed surfactant (**2**) was also prepared to investigate the effect of alkyl corona on the ICRM's property (*vide infra*). It should be mentioned that, although double-tailed surfactants (*e.g.*, AOT) are commonly used to form RMs,[26,27] single-tailed surfactants such as SDS (sodium dodecyl sulfate)[27] and CTAB are able to do the same under appropriate conditions.[56]

Cross-linking of the RMs was achieved by UV irradiation of the solution (W_0 = 5) in the presence of 2,2′-dimethoxy-2-phenylacetophenone, a photoinitiator (Scheme 1). After cross-linking, the sharp peaks in the ^{1}H NMR spectrum of a 2:3 mixture of **1** and DTT (Figure 1a) became broad and the alkenic protons of **1** and those on the cross-linker disappeared almost completely (Figure 1b). We chose the 2:3 stoichiometry because the surfactant has three alkenyl groups and the cross-linker two thiols. The reaction was fast, but a small percentage of the alkenyl groups remained even after 10 h of UV irradiation. After evaporation of solvents and washing with water, the materials obtained were soluble in common organic solvents such as chloroform and tetrahydrofuran but insoluble in polar protic solvents such as water and methanol or highly nonpolar solvent such as hexane. Notably, the methyl and methylene protons of the dodecyl chain were sharp and well-resolved in the ^{1}H NMR spectrum of the materials, whereas the protons near the ammonium headgroup were broad and weak/absent (Figure 1c). These results are consistent with cross-linking at the interface in the RM configuration, which constrains the movement of the ammonium headgroup but not that of the hydrocarbon tails pointing outward.

Characterization of ICRMs. The ICRMs were characterized additionally by dynamic light scattering (DLS) and transmission electron microscopy (TEM). Table 1 summarizes the hydrodynamic diameters of the RMs and ICRMs determined in various solvents. The RMs were captured in 2:1 heptane/$CHCl_3$. Instead of trying to obtain the refractive index and viscosity for the mixed solvent, we calculated the diameter of the RMs using the parameters of heptane (entry 1) and $CHCl_3$ (entry 2), respectively.[57] The sizes (5−6 nm) obtained were indeed very close and compared favorably with those of conventional AOT RMs (2−3 nm),[26] considering the (longer) dodecyl tail of **1** and the extra phenylene spacer.

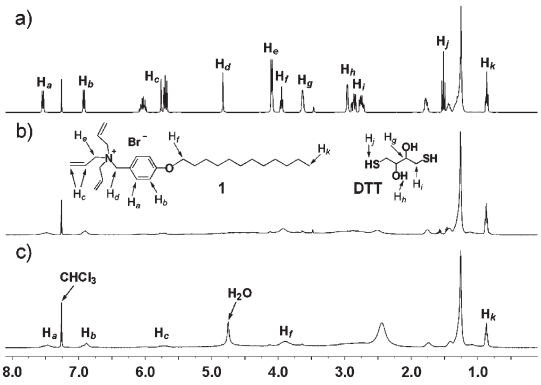

Figure 1. ^{1}H NMR spectra of a 2:3 mixture of 1 and DTT (a) before irradiation, (b) after UV irradiation for 10 h, and (c) after washing with H_2O.

TABLE 1. Hydrodynamic Diameters of RMs and ICRMs Determined by DLS[a]

entry	sample	solvent	diameter (nm)
1	RMs of **1**	2:1 heptane/$CHCl_3$	6[b]
2	RMs of **1**	2:1 heptane/$CHCl_3$	5[c]
3	ICRMs of **1**	$CHCl_3$	190
4	ICRMs of **1**	THF	13
5	RMs of **2**	2:1 heptane/$CHCl_3$	5[b]
6	RMs of **2**	2:1 heptane/$CHCl_3$	4[c]
7	ICRMs of **2**	$CHCl_3$	5
8	ICRMs of **2**	THF	4

[a] The diameters were averages of five measurements. Each measurement was based on 20 accumulations of data collection. The relative standard deviations within the five measurements ranged from 1 to 9%. [b] The diameter was calculated using the viscosity and refractive index of heptane. [c] The diameter was calculated using the viscosity and refractive index of $CHCl_3$.

The size of the ICRMs of **1** obtained by DLS strongly depended upon the solvent. The particle size averaged *ca.* 190 nm in $CHCl_3$ but only 13 nm in THF (Table 1, entries 3 and 4). It is certainly possible that some coalescence occurred during cross-linking, and the resulting ICRMs were larger than the original RMs, as reported in some of McQuade's examples.[32] The huge change of size in different solvents, however, indicates that the cross-linked materials (whether in the desired form of ICRMs or something else) aggregated in a solvent-dependent manner.

Surfactant **1** was soluble in many organic solvents, including methanol, chloroform, and THF. The materials obtained after cross-linking remained soluble in chloroform and THF but were insoluble in methanol.

The result was expected of the configuration of ICRMs, whose alkyl chains are oriented outward. TEM results (*vide infra*) also suggested successful capture of the RMs. It is perplexing, nonetheless, that the ICRMs, being completely hydrophobic on the outside, could aggregate in chloroform.

For good solubility, solvent−particle interactions must be able to overcome the particle−particle interactions. Strong interparticulate interactions lead to aggregation and, ultimately, insolubility. Unlike self-assembled RMs whose components (surfactants and entrapped water) can exchange rapidly, ICRMs are covalently fixed macromolecules. Because a macromolecule gains much less entropy when going into the solution phase, its dissolution is more difficult than its small-molecule components.[58] The ICRMs can interact with one another through van der Waals interactions of the alkyl chains on the surface. Their cores consist of charged ammonium headgroups, and aggregation thus can benefit as well from electrostatic interactions, which could operate over a long distance.

The best solvents are apparently those with intermediate polarity, such as chloroform and THF. Neither highly polar (methanol and water) nor highly nonpolar (hexane) solvents dissolved the ICRMs. We also studied the ICRMs of **1** in acetone and butanone. The particles dissolved readily in butanone, but dissolution in acetone required gentle heating. The average hydrodynamic diameter was about 30 nm in both solvents for freshly made samples (Figures 1S and 2S in Supporting Information) at 25 °C. Over 1−2 h, however, the scattering intensity increased significantly for the acetone sample and large particles, micrometers in size, began to form (Figure 3S). These large particles eventually became insoluble in acetone and precipitated out of the solution, at which time the scattering intensity became extremely low. On the other hand, the size in butanone was stable over time. Most likely, acetone lies in between butanone and methanol with regard to its ability to dissolve the ICRMs—although dissolution is possible with heating, aggregation is so strong at room temperature that the particles eventually precipitate out of the solution.

Given the bulkiness of the benzyltriallylammonium headgroup, the surface density of alkyl chains for the ICRMs of **1** is quite limited. When the ICRMs approach one another, the alkyl chains from different particles can interdigitate, greatly enhancing the van der Waals interactions among the alkyl groups (Figure 2, left). Aggregation and alkyl interdigitation thus can fill the "gaps" in the ICRM shell in a highly efficient manner. The same process can also release entrapped solvent molecules between the alkyl chains—an entropically favorable process. As the nanoparticles get closer, electrostatic interactions among the ICRM cores would increase, making the aggregation even more energetically advantageous.

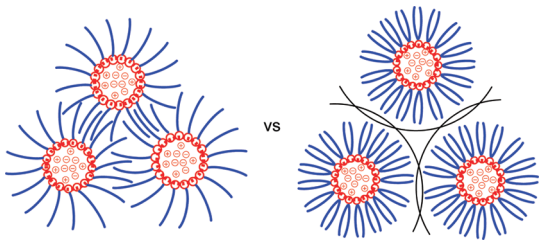

Figure 2. Schematic representation of the aggregational mechanism.

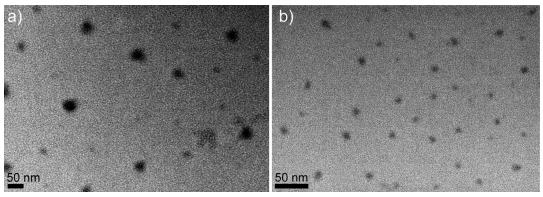

Figure 3. TEM micrographs of the ICRMs from (a) 1 and (b) 2. The samples were prepared by evaporating a THF solution of the ICRMs.

If the above hypothesis is correct, the best way to prevent the aggregation is probably to increase the alkyl density on the ICRM surface (Figure 2, right). We thus prepared the double-tailed **2** and obtained ICRMs following similar procedures. ^{1}H NMR spectroscopy once again showed disappearance/weakening of protons near the headgroup and sharp, well-resolved peaks for the alkyl tails (Figure 4S). The cross-linking reaction seemed to be more complete in the double-tailed surfactant, as judged by the amount of residual alkenic proton in Figures 1c and 4S. It is possible that the conical shape of the double-tailed surfactant makes its RMs more stable[59] and facilitated the intramicellar thiol−ene reaction. Most importantly, the RMs of **2** have identical sizes (4−5 nm in diameter) before and after cross-linking, independent of solvents (Table 1, entries 5−8). As expected, with an increase in the alkyl density at the exterior, the nanoparticles became even less soluble in polar solvents. The ICRMs of **2**, for example, were completely insoluble in acetone even upon heating.

TEM allows us to directly visualize the ICRMs. Negative staining with phosphotungstic acid afforded good images in the case of ICRMs of **1** (Figure 5S) but caused severe aggregation in the ICRMs of **2** (data not shown). McQuade reported similar behavior for their cross-linked RMs.[32] Fortunately, both surfactants have a bromide counteranion; its electron density was high enough to enable us to image the nanoparticles without any staining, albeit the contrast was not ideal (Figure 3). The results were consistent with those from the DLS. For the ICRMs of **1**, both small (diameter ≈10 nm) and large particles (diameter ≈50 nm) could be found in a sample prepared from THF. The large ones could be aggregates of the small ones, as suggested by the DLS study. It is also possible that some

large particles might result from coalescence of RMs during cross-linking and thus were permanent. We were not sure whether the slightly lower cross-linking in the RMs of **1** also contributed to the aggregation. Importantly, the ICRMs of the double-tailed surfactant were much smaller (Figure 3b), with the majority of the particles 5−7 nm in diameter, completely in line with the DLS sizes (Table 1).

Template Synthesis of Metal Nanoparticles with ICRMs with $NaBH_4$ as the Reducing Agent. With introverted ammonium groups at the core, the ICRMs should be particularly suitable for template synthesis with anionic metal precursors. Indeed, these organic nanoparticles easily extracted tetrachloroaurate ($AuCl_4^-$) from water to chloroform. Addition of $NaBH_4$ to the chloroform solution immediately turned its color from light yellow to dark purple.

When an equivalent amount of aurate was used (*i.e.*, $[AuCl_4^-]/[\mathbf{1}] = 1$), the UV−vis spectrum showed broad absorption with a peak at 520 nm (Figure 4, red), indicating the formation of gold nanoparticles >2 nm in diameter.[60−62] The solution was stable indefinitely in our hands, showing no signs of precipitation and/or aggregation. The surface plasmon absorption band at 520 nm became significantly weaker, and a higher-energy peak appeared at *ca.* 330 nm when the $[AuCl_4^-]/[\mathbf{1}]$ was reduced to 0.1, indicating formation of both large (>2 nm)[60−62] and ultrasmall (<1 nm)[37] nanoparticles under this condition (Figure 4, green). The amount of ultrasmall nanoparticles increased even more as the $[AuCl_4^-]/[\mathbf{1}]$ ratio was reduced to 0.02. The absorption at 330 nm became stronger, and that at 520 disappeared completely (Figure 4, blue). Notably, the size of the gold nanoparticles seemed to be mainly controlled by the amount of aurate. Different amounts of water ($W_0 = 1$ or 5), which controlled the size of the water droplet in the RM, for example, caused very little difference in the position of the absorption (compare the blue and violet spectra in Figure 4). The results indicated that the template synthesis was mainly controlled by the stoichiometry of the reactants. Template synthesis using the ICRMs of **2** gave similar results. Only the sample with $[AuCl_4^-]/[\mathbf{2}] = 1$, for example, gave strong surface plasmon band (Figure 6S).

The conclusions from the UV studies were confirmed by TEM. The particles obtained at $[AuCl_4^-]/[\mathbf{1}] = 1$ averaged about 3 nm in diameter (Figure 5a). Similar-sized nanoparticles were also observed at $[AuCl_4^-]/[\mathbf{1}] = 0.1$, but far fewer particles appeared in the micrograph even though the concentration of the TEM sample in Figure 5b was much higher than what was used in Figure 5a. Presumably, subnanometer gold particles existed in sample 4b but could not be detected by TEM. This trend continued as $[AuCl_4^-]/[\mathbf{1}]$ was reduced to 0.02. Even fewer particles were observable in TEM and what could be seen were very small (1 nm or less), as shown by Figure 5c.

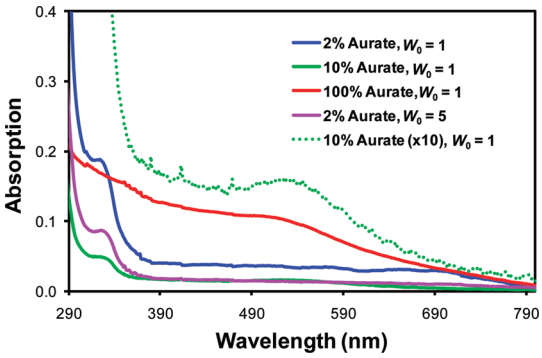

Figure 4. UV−vis spectra of Au-ICRMs prepared with $[AuCl_4^-]/[1] = 1$, 0.1, and 0.02. The dotted green spectrum was that from $[AuCl_4^-]/[1] = 0.1$ multiplied by 10. $[1] = 5 \times 10^{-4}$ M.

Subnanometer gold and silver clusters attracted much interest in recent years as novel biolabels and optoelectronic emitters.[37−47] As their size approaches the Fermi wavelength of electrons, noble metal clusters display dramatically different optical, electronic, and chemical properties from either bulk or nanoscale metals. The photoluminescence of these materials agreed completely with the UV−vis and TEM data. Under a hand-held UV lamp (365 nm), the Au-ICRMs prepared with $[AuCl_4^-]/[\mathbf{1}] = 1$ gave no signs of luminescence (Figure 5a, inset). As the $[AuCl_4^-]/[\mathbf{1}]$ ratio decreased, the sample became increasingly fluorescent, with the sample prepared with the 2 mol % aurate giving the brightest blue light (Figure 5c, inset).

A unique property of subnanometer gold clusters is their atom-like properties.[37−47] Indeed, the excitation/emission spectra of these Au-ICRMs resembled those of molecular fluorophores, displaying the maximum at 315/354 nm (Figure 6, blue). The electronic transition energy of Au clusters is known to scale with inverse cluster radius.[37] The excitation/emission wavelengths for Au_3, Au_4, and Au_5 clusters, for example, were reported to be 305/340,[63] 313/371,[40] and 330/385 nm,[64] respectively. Comparison with the literature data suggests that the dominant fluorescent species in our Au-ICRMs is probably Au_4, a reasonable result based on the amount of aurate used in the synthesis.

Nanoalloys such as Au−Pt could be easily prepared *via* our template synthesis. Using $PtCl_6^{2-}$ or a 1:1 mixture of $AuCl_4^-$ and $PtCl_6^{2-}$, we obtained fluorescent Pt and Au−Pt clusters starting with 2 mol % of the total metal precursor. The excitation/emission wavelengths of the Pt clusters were 346/399 nm (Figure 6, red). Interestingly, the Au−Pt clusters displayed an intermediate values (329/390 nm, Figure 6, green). It seems that the few metal atoms indeed existed as an alloy instead of separate clusters.

Template Synthesis of Metal Nanoparticles with ICRMs without Externally Added Reducing Agents. We were puzzled by the nanometer-sized gold nanoparticles formed in the template synthesis with 100% aurate loading. Even if

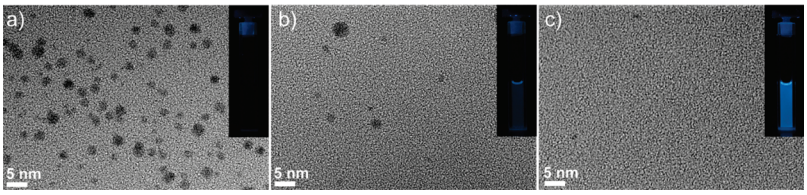

Figure 5. TEM micrographs of Au-ICRMs with (a) 1:1, (b) 0.1:1, and (c) 0.02:1 [$HAuCl_4$]/[1]. The gold nanoparticles appear as dark spots due to their high electron density. The insets are the corresponding photographs of Au-ICRMs under a hand-held UV lamp (365 nm).

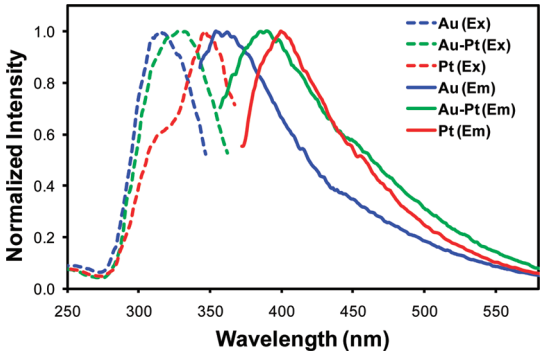

Figure 6. Excitation (dotted lines) and emission spectra (solid lines) of Au, Au−Pt, and Pt nanoparticles prepared with ICRM templates.

the hydrophilic core of an ICRM was large enough to accommodate the metal nanoparticle, a single ICRM should not contain enough aurate ions to produce a 3 nm diameter gold particle, which should consist of approximately 1000 gold atoms.[60] The only possible way to form such a large gold nanoparticle was for gold atoms from many ICRMs to merge. The gold migration and agglomeration should not be caused by the aggregation or the somewhat lower cross-linking density of the RMs of **1**, as the same happened to the RMs of **2**, which showed no aggregation and higher cross-linking. The core of our ICRM mostly consists of thioether and hydroxyl groups. If a large number of gold atoms form quickly upon reduction with $NaBH_4$, lack of proper surface stabilization might be the reason for the gold migration and agglomeration. After all, gold migration and agglomeration are norm rather than exceptions whenever the metal surface is not properly protected. This is why reduction of aurate tends to give bulk gold precipitate unless proper surface passivation is present.[65]

With the above hypothesis, we decided to attempt slow reduction of the entrapped aurate. Remarkably, when the aurate-containing ICRMs were allowed to sit at room temperature without any $NaBH_4$ added, the sample became luminescent and turned from yellow (the distinctive color of aurate) to colorless in a few hours. Thiols were reported to reduce aurate, although not all thiols were able to do the same.[66] DTT is a widely used reducing thiol in biology and in our hands could reduce aurate in water.[67] ^{1}H NMR spectroscopy indicated that free DTT was not present in our sample—the ICRMs were generally washed extensively with water before the template synthesis. Although some residual thiols possibly could be left at the core of the ICRMs if they become geometrically isolated during the cross-linking, IR spectroscopy (Figure 7S) showed no peaks around 2550 cm^{-1}, indicating little if any residual thiol was present.

The entrapped aurate ions seemed to be completely reduced under our experimental conditions. Addition of extra DTT or hydrazine, for example, changed neither the color of the Au-ICRMs nor their luminescence once they were formed. The samples with 2% aurate emit blue light, the same as those reduced with excess $NaBH_4$. Moreover, when the ICRMs in chloroform were stirred with a large excess of aurate (>50 equiv) in the aqueous phase, the aurate was extracted continuously into the organic phase and reduced. The luminescence disappeared, and the solution turned brown, indicative of larger particles.

Tetrachloroaurate is a strong oxidizing agent. Spontaneous reduction of aurate has been reported in the literature, typically in the presence of a polymer or dendrimer. Hydroxyl,[68,69] ether,[68,70−72] or amide[73] were all found to reduce aurate at room temperature without any externally added reductant. The ICRMs contain ether, hydroxyl, thioether, and bromide counteranions; all are potential reducing agents. It is not exactly clear what the reducing agent was in our system, as the IR spectra of the ICRMs and Au-ICRMs were very similar (Figure 7S). We did not see obvious oxidized products such as ketone or carboxylic acid by the IR spectroscopy. The spontaneous reduction of aurate was reported to be assisted by its dehydration within block copolymer micelles[74] or encapsulation within dendrimers.[72] Although structurally different from these polymeric micelles and dendrimers, the ICRMs were essentially doing the same (*i.e.*, dehydration and encapsulation) as they extracted the aurate from the aqueous phase to their interior.

In the absence of $NaBH_4$, the gold clusters formed within the ICRMs were no longer prone to migration and agglomeration. UV−vis spectroscopy showed no surface plasmon absorption even when 1 equiv of aurate was used in the template synthesis. The Au-ICRM samples, with [$HAuCl_4$]/[**1**] from 0.02 to 0.1 to 1, all

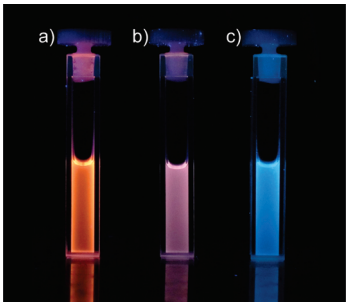

Figure 7. Photographs of Au-ICRMs prepared with $[HAuCl_4]/[1]$ = (a) 1:1, (b) 0.1:1, and (c) 0.02:1 under a hand-held UV lamp (365 nm). The gold nanoparticles were formed without externally added reducing agents.

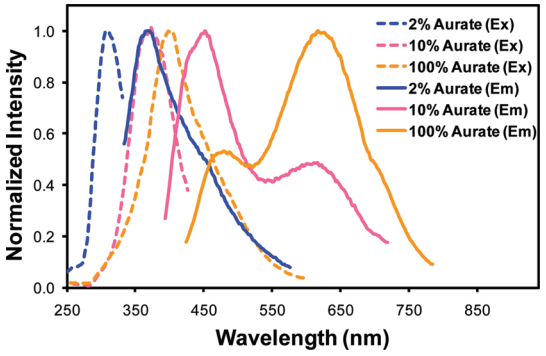

Figure 8. Excitation (dotted lines) and emission spectra (solid lines) of Au-ICRMs prepared with $[AuCl_4^-]/[1]$ = 1, 0.1, and 0.02. The gold nanoparticles were formed without externally added reducing agents.

became luminescent (Figure 7). The excitation/emission wavelengths for the 2% aurate sample (blue) was 308/368 nm (Figure 8), very similar to those of the Au_4 clusters obtained from $NaBH_4$ reduction. The 10% aurate sample (pink) had the maximum excitation wavelength at 375 nm, similar to what was reported for Au_8 clusters in the literature.[64] The emission spectrum showed two maxima at 451 and 622 nm, with the former being stronger. Au_8 clusters were reported to emit at 456 nm.[64] The extra peak at 622 nm must come from a small population of larger gold clusters formed in the synthesis. When 1 equiv of aurate was used in the template synthesis, the maximum excitation wavelength shifted to 403 nm and two maxima (at 478 and 617 nm) appeared in the emission spectra. We were not able to find the exact matching of our data in the literature, but the major emission at 617 nm suggests that the size of the cluster was between Au_{13} and Au_{23}, assuming the ligands on the surface do not have a significant effect on the luminescent properties.[37] Template syntheses with the ICRMs of **2** gave very similar results, except the emission spectra showed more homogeneous Au particle formation (Figure 8S).

CONCLUSIONS

The thiol−ene reaction indeed is well-suited for the covalent capture of RMs. The combination of a surfactant with a triallylammonium headgroup and a hydrophilic thiol cross-linker directs the cross-linking to the surfactant−water interface. The efficiency of the reaction is enhanced when the hydrophilic cross-linker is concentrated into the water pool inside the RMs. Although the ICRMs from the single-tailed surfactant are soluble in many organic solvents, the particles aggregate extensively, as the alkyl chains from different ICRMs could interdigitate. Aggregation is probably driven by a combination of van der Waals interactions among the alkyl chains and electrostatic interactions among the charged cores. Consistent with the hypothesis, the ICRMs of the double-tailed surfactant do not aggregate and are identical in size compared to the RMs prior to cross-linking.

Importantly, the ICRMs can extract metal salts easily into their hydrophilic core, making them ideal templates for nanoparticle synthesis. Although gold and platinum nanoparticles were prepared in this work, the general concept is applicable to other materials. The stability of conventional gold nanoparticles derives from surface passivation.[60−62,75] In our synthesis, the gold particles/clusters are protected physically and at most by weak ligands such as thiolether, bromide, and hydroxyl groups. The straightforward preparation of the cross-linkable surfactants, the simplicity of the template synthesis, and the many potential applications of the noble metal clusters likely will make the ICRMs highly attractive templates in advanced nanomaterials synthesis.

MATERIALS AND METHODS

General. All reagents and solvents were of ACS certified grade or higher and were used as received from commercial suppliers. Routine ^1H and ^{13}C NMR spectra were recorded on a Varian VXR-400 and Bruker DRX-400 spectrometer. ESI-MS was performed on a FINNIGAN TSQ700 mass spectrometer. DLS studies were performed on a PDDLS/Cool Batch 90 T dynamic light scattering detector at 25.0 °C. The intensity data were analyzed with the PRECISION DECONVOLVE program, and the size measurement was based on five replicates. Fluorescence spectra were recorded at ambient temperature on a Varian Cary Eclipse fluorescence spectrophotometer. Transmission electron microscopy (TEM) studies were carried out on a PHILIPS CM 30 instrument, operating at 150 kV for ICRMs and 200 kV for Au nanoparticles, separately.

Chemicals. Syntheses of **1** and **2** are reported in the Supporting Information.

Typical Preparation of ICRMs. Water (1.8 μL) was added to a solution of **1** (9.8 mg, 0.02 mmol) in heptane (1.0 mL) and $CHCl_3$ (0.5 mL). The mixture was hand shaken and sonicated at room

temperature for 1 min to give an optically clear solution. After addition of DTT (4.6 mg, 0.03 mmol) and 2,2′-dimethoxy-2-phenylacetophenone (25.6 mg/10 mL in chloroform, 10 μL, 0.1 μmol), the mixture was irradiated in a Rayonet photoreactor for *ca.* 10 h until most alkenic protons in **1** were consumed. The organic solvents were removed by rotary evaporation and the residue was washed by water to give a white power (11.2 mg).

Typical Preparation of Au-ICRMs with $NaBH_4$ as the Reducing Agent. A 10 mM aqueous solution of $HAuCl_4$ (2 mL) was added to a 10 mM IRCM solution (W_0 = 1 or 5) in chloroform (2 mL). The aqueous phase became colorless, and the organic phase turned yellow upon stirring. A freshly prepared aqueous solution of sodium borohydride (0.2 M, 1 mL) was slowly added to the vigorously stirred reaction mixture. The organic phase turned purple immediately, and the color intensified over 2 h. The organic phase was washed with water three times and concentrated by rotary evaporation. The residue could be redissolved in common organic solvents and was stable over a period of several months.

Typical Preparation of Au-ICRMs without Externally Added Reducing Agents. A 10 mM aqueous solution of $HAuCl_4$ (2 mL) was added to a 10 mM IRCM solution (W_0 = 5) in chloroform (2 mL). The aqueous phase became colorless, and the organic phase turned yellow upon stirring. Upon sitting at room temperature overnight, the organic phase became colorless. The organic phase was separated, washed with water three times, and concentrated by rotary evaporation. The residue could be redissolved in common organic solvents and was stable over a period of several months.

Acknowledgment. We thank NSF (CHE-0748616) for supporting this research.

Supporting Information Available: Synthetic procedures, additional DLS, UV, and fluorescence data (PDF). This material is available free of charge *via* the Internet at http://pubs.acs.org.

REFERENCES AND NOTES

1. Mueller, A.; O'Brien, D. F. Supramolecular Materials *via* Polymerization of Mesophases of Hydrated Amphiphiles. *Chem. Rev.* **2002,** *102*, 727–757.
2. Gin, D. L.; Gu, W.; Pindzola, B. A.; Zhou, W. J. Polymerized Lyotropic Liquid Crystal Assemblies for Materials Applications. *Acc. Chem. Res.* **2001,** *34*, 973–980.
3. Eastoe, J.; Summers, M.; Heenan, R. K. Control over Phase Curvature Ssing Mixtures of Polymerizable Surfactants. *Chem. Mater.* **2000,** *12*, 3533–3537.
4. Yan, F.; Texter, J. Polymerization of and in Mesophases. *Adv. Colloid Interface Sci.* **2006,** *128−130*, 27–35.
5. Tajima, K.; Aida, T. Controlled Polymerizations with Constrained Geometries. *Chem. Commun.* **2000,** 2399–2412.
6. Larrabee, C. E.; Sprague, E. D. Radiation-Induced Polymerization of Sodium 10-Undecenoate in Aqueous Micelle Solutions. *J. Polym. Sci., Part C: Polym. Lett.* **1979,** *17*, 749–757.
7. Paleos, C. M.; Stassinopoulou, C. I.; Malliaris, A. Comparative Studies between Monomeric and Polymeric Sodium 10-Undecenoate Micelles. *J. Phys. Chem.* **1983,** *87*, 251–254.
8. Joynes, D.; Sherrington, D. C. Novel Polymerizable Mono- and Divalent Quaternary Ammonium Cationic Surfactants 1. Synthesis, Structural Characterization and Homopolymerization. *Polymer* **1996,** *37*, 1453–1462.
9. Dais, P.; Paleos, C. M.; Nika, G.; Malliaris, A. Positional Effects of the Methacrylate Group on Polymerization and Microstructure of Micelle-Forming Quaternary Ammonium-Salts Studied by NMR-Spectroscopy. *Makromol. Chem.* **1993,** *194*, 445–450.
10. Ringsdorf, H.; Schlarb, B.; Venzmer, J. Molecular Architecture and Function of Polymeric Oriented Systems: Models for the Study of Organization, Surface Recognition, and Dynamics of Biomembranes. *Angew. Chem., Int. Ed. Engl.* **1988,** *27*, 113–158.
11. Fendler, J. H.; Tundo, P. Polymerized Surfactant Aggregates—Characterization and Utilization. *Acc. Chem. Res.* **1984,** *17*, 3–8.
12. Higashi, N.; Adachi, T.; Niwa, M. A Novel 2-Dimensional Photopolymerization at an Oriented Bilayer Surface—Effective Molecular-Weight Control Using Membrane State and Chain Transfer. *Macromolecules* **1990,** *23*, 1475–1480.
13. Fukuda, H.; Diem, T.; Stefely, J.; Kezdy, F. J.; Regen, S. L. Polymer-Encased Vesicles Derived from Dioctadecyldimethylammonium Methacrylate. *J. Am. Chem. Soc.* **1986,** *108*, 2321–2327.
14. Sisson, T. M.; Srisiri, W.; O'Brien, D. F. Novel Polymer Architectures *via* the Selective Polymerization of Lyotropic Liquid Crystals of Heterobifunctional Amphiphiles. *J. Am. Chem. Soc.* **1998,** *120*, 2322–2329.
15. Srisiri, W.; Sisson, T. M.; OBrien, D. F.; McGrath, K. M.; Han, Y. Q.; Gruner, S. M. Polymerization of the Inverted Hexagonal phase. *J. Am. Chem. Soc.* **1997,** *119*, 4866–4873.
16. Deng, H.; Gin, D. L.; Smith, R. C. Polymerizable Lyotropic Liquid Crystals Containing Transition-Metal and Lanthanide Ions: Architectural Control and Introduction of New Properties into Nanostructured Polymers. *J. Am. Chem. Soc.* **1998,** *120*, 3522–3523.
17. Reppy, M. A.; Gray, D. H.; Pindzola, B. A.; Smithers, J. L.; Gin, D. L. A New Family of Polymerizable Lyotropic Liquid Crystals: Control of Feature Size in Cross-Linked Inverted Hexagonal Assemblies *via* Monomer Structure. *J. Am. Chem. Soc.* **2001,** *123*, 363–371.
18. Smith, R. C.; Fischer, W. M.; Gin, D. L. Ordered Poly(*p*-phenylenevinylene) Matrix Nanocomposites *via* Lyotropic Liquid-Crystalline Monomers. *J. Am. Chem. Soc.* **1997,** *119*, 4092–4093.
19. Kerr, R. L.; Miller, S. A.; Shoemaker, R. K.; Elliott, B. J.; Gin, D. L. New Type of Li Ion Conductor with 3D Interconnected Nanopores *via* Polymerization of a Liquid Organic Electrolyte-Filled Lyotropic Liquid-Crystal Assembly. *J. Am. Chem. Soc.* **2009,** *131*, 15972–15973.
20. Lee, Y. S.; Yang, J. Z.; Sisson, T. M.; Frankel, D. A.; Gleeson, J. T.; Aksay, E.; Keller, S. L.; Gruner, S. M.; Obrien, D. F. Polymerization of Nonlamellar Lipid Assemblies. *J. Am. Chem. Soc.* **1995,** *117*, 5573–5578.
21. Yang, D.; O'Brien, D. F.; Marder, S. R. Polymerized Bicontinuous Cubic Nanoparticles (Cubosomes) from a Reactive Monoacylglycerol. *J. Am. Chem. Soc.* **2002,** *124*, 13388–13389.
22. Yang, D.; Armitage, B.; Marder, S. R. Cubic Liquid-Crystalline Nanoparticles. *Angew. Chem., Int. Ed.* **2004,** *43*, 4402–4409.
23. Gray, D. H.; Hu, S. L.; Juang, E.; Gin, D. L. Highly Ordered Polymer−Inorganic Nanocomposites *via* Monomer Self-Assembly: *In Situ* Condensation Approach. *Adv. Mater.* **1997,** *9*, 731–736.
24. Zhou, M. J.; Kidd, T. J.; Noble, R. D.; Gin, D. L. Supported Lyotropic Liquid-Crystal Polymer Membranes: Promising Materials for Molecular-Size-Selective Aqueous Nanofiltration. *Adv. Mater.* **2005,** *17*, 1850–1853.
25. Gin, D. L.; Lu, X. Y.; Nemade, P. R.; Pecinovsky, C. S.; Xu, Y. J.; Zhou, M. J. Recent Advances in the Design of Polymerizable Lyotropic Liquid-Crystal Assemblies for Heterogeneous Catalysis and Selective Separations. *Adv. Funct. Mater.* **2006,** *16*, 865–878.
26. Fendler, J. H. *Membrane Mimetic Chemistry: Characterizations and Applications of Micelles, Microemulsions, Monolayers, Bilayers, Vesicles, Host−Guest Systems, and Polyions*; Wiley: New York, 1982.
27. Pileni, M. P. *Structure and Reactivity in Reverse Micelles*; Elsevier: Amsterdam, 1989.
28. Pileni, M. P. Nanosized Particles Made in Colloidal Assemblies. *Langmuir* **1997,** *13*, 3266–3276.
29. Pileni, M. P. The Role of Soft Colloidal Templates in Controlling the Size and Shape of Inorganic Nanocrystals. *Nat. Mater.* **2003,** *2*, 145–150.

30. Voortmans, G.; De Schryver, F. C. Polymerization in and of Inverse Micelles. In *Structure and Reactivity in Reverse Micelles*; Pileni, M. P., Ed.; Elsevier: Amsterdam, 1989.
31. Voortmans, G.; Verbeeck, A.; Jackers, C.; Deschryver, F. C. Polymerization of *N*,*N*-Didodecyl-*N*-methyl-*N*-(2-(methacryloyloxy)ethyl)ammonium Chloride, an Inverse Micelle Forming Detergent. *Macromolecules* **1988,** *21*, 1977–1980.
32. Jung, H. M.; Price, K. E.; McQuade, D. T. Synthesis and Characterization of Cross-Linked Reverse Micelles. *J. Am. Chem. Soc.* **2003,** *125*, 5351–5355.
33. Price, K. E.; McQuade, D. T. A Cross-Linked Reverse Micelle-Encapsulated Palladium Catalyst. *Chem. Commun.* **2005,** 1714–1716.
34. Dondoni, A. The Emergence of Thiol−Ene Coupling as a Click Process for Materials and Bioorganic Chemistry. *Angew. Chem., Int. Ed.* **2008,** *47*, 8995–8997.
35. Hoyle, C. E.; Lee, T. Y.; Roper, T. Thiol-Enes: Chemistry of the Past with Promise for the Future. *J. Polym. Sci., Part A: Polym. Chem.* **2004,** *42*, 5301–5338.
36. Iha, R. K.; Wooley, K. L.; Nystrom, A. M.; Burke, D. J.; Kade, M. J.; Hawker, C. J. Applications of Orthogonal "Click" Chemistries in the Synthesis of Functional Soft Materials. *Chem. Rev.* **2009,** *109*, 5620–5686.
37. Zheng, J.; Nicovich, P. R.; Dickson, R. M. Highly Fluorescent Noble-Metal Quantum Dots. *Annu. Rev. Phys. Chem.* **2007,** *58*, 409–431.
38. Zheng, J.; Petty, J. T.; Dickson, R. M. High Quantum Yield Blue Emission from Water-Soluble Au_8 Nanodots. *J. Am. Chem. Soc.* **2003,** *125*, 7780–7781.
39. Negishi, Y.; Takasugi, Y.; Sato, S.; Yao, H.; Kimura, K.; Tsukuda, T. Magic-Numbered Au(*n*) Clusters Protected by Glutathione Monolayers (*n* = 18, 21, 25, 28, 32, 39): Isolation and Spectroscopic Characterization. *J. Am. Chem. Soc.* **2004,** *126*, 6518–6519.
40. Tran, M. L.; Zvyagin, A. V.; Plakhotnik, T. Synthesis and Spectroscopic Observation of Dendrimer-Encapsulated Gold Nanoclusters. *Chem. Commun.* **2006,** 2400–2401.
41. Duan, H.; Nie, S. Etching Colloidal Gold Nanocrystals with Hyperbranched and Multivalent Polymers: A New Route to Fluorescent and Water-Soluble Atomic Clusters. *J. Am. Chem. Soc.* **2007,** *129*, 2412–2413.
42. Xie, J.; Zheng, Y.; Ying, J. Y. Protein-Directed Synthesis of Highly Fluorescent Gold Nanoclusters. *J. Am. Chem. Soc.* **2009,** *131*, 888–889.
43. Zheng, J.; Dickson, R. M. Individual Water-Soluble Dendrimer-Encapsulated Silver Nanodot Fluorescence. *J. Am. Chem. Soc.* **2002,** *124*, 13982–13983.
44. Zhang, J. G.; Xu, S. Q.; Kumacheva, E. Photogeneration of Fluorescent Silver Nanoclusters in Polymer Microgels. *Adv. Mater.* **2005,** *17*, 2336–2340.
45. Shen, Z.; Duan, H. W.; Frey, H. Water-Soluble Fluorescent Ag Nanoclusters Obtained from Multiarm star Poly(acrylic acid) as "Molecular Hydrogel" Templates. *Adv. Mater.* **2007,** *19*, 349–352.
46. Zheng, J.; Ding, Y.; Tian, B. Z.; Wang, Z. L.; Zhuang, X. W. Luminescent and Raman Active Silver Nanoparticles with Polycrystalline Structure. *J. Am. Chem. Soc.* **2008,** *130*, 10472–10473.
47. Maretti, L.; Billone, P. S.; Liu, Y.; Scaiano, J. C. Facile Photochemical Synthesis and Characterization of Highly Fluorescent Silver Nanoparticles. *J. Am. Chem. Soc.* **2009,** *131*, 13972–13980.
48. Lee, H.; Habas, S. E.; Kweskin, S.; Butcher, D.; Somorjai, G. A.; Yang, P. Morphological Control of Catalytically Active Platinum Nanocrystals. *Angew. Chem., Int. Ed.* **2006,** *45*, 7824–7828.
49. Narayanan, R.; El-Sayed, M. A. Effect of Catalysis on the Stability of Metallic Nanoparticles: Suzuki Reaction Catalyzed by PVP−Palladium Nanoparticles. *J. Am. Chem. Soc.* **2003,** *125*, 8340–8347.
50. Tian, N.; Zhou, Z. Y.; Sun, S. G.; Ding, Y.; Wang, Z. L. Synthesis of Tetrahexahedral Platinum Nanocrystals with High-Index Facets and High Electro-oxidation Activity. *Science* **2007,** *316*, 732–735.
51. Wang, C.; Daimon, H.; Lee, Y.; Kim, J.; Sun, S. Synthesis of Monodisperse Pt Nanocubes and Their Enhanced Catalysis for Oxygen Reduction. *J. Am. Chem. Soc.* **2007,** *129*, 6974–6975.
52. Tsung, C. K.; Kuhn, J. N.; Huang, W.; Aliaga, C.; Hung, L. I.; Somorjai, G. A.; Yang, P. Sub-10 nm Platinum Nanocrystals with Size and Shape Control: Catalytic Study for Ethylene and Pyrrole Hydrogenation. *J. Am. Chem. Soc.* **2009,** *131*, 5816–5822.
53. Killops, K. L.; Campos, L. M.; Hawker, C. J. Robust, Efficient, and Orthogonal Synthesis of Dendrimers *via* Thiol−Ene "Click" Chemistry. *J. Am. Chem. Soc.* **2008,** *130*, 5062–5064.
54. Chan, J. W.; Hoyle, C. E.; Lowe, A. B. Sequential Phosphine-Catalyzed, Nucleophilic Thiol−Ene/Radical-Mediated Thiol−Yne Reactions and the Facile Orthogonal Synthesis of Polyfunctional Materials. *J. Am. Chem. Soc.* **2009,** *131*, 5751–5753.
55. Floyd, N.; Vijayakrishnan, B.; Koeppe, A. R.; Davis, B. G. Thiyl Glycosylation of Olefinic Proteins: S-Linked Glycoconjugate Synthesis. *Angew. Chem., Int. Ed.* **2009,** *48*, 7798–7802.
56. Cuccovia, I. M.; Dias, L. G.; Maximiano, F. A.; Chaimovich, H. Analysis of the Bromide Ion Distribution in the Water Pool of Reverse Micelles of Hexadecyltrimethylammonium Bromide in Chloroform/*n*-Dodecane and Isooctane/*n*-Hexanol by Chemical Trapping. *Langmuir* **2001,** *17*, 1060–1068.
57. The refractive index for heptane and $CHCl_3$ at 25 °C is 1.3855 and 1.4422, and the viscosity is 0.386 and 0.54 cP, respectively.
58. Flory, P. J. *Principles of Polymer Chemistry*; Cornell University Press: Ithaca, NY, 1953; pp 495−503.
59. Israelachvili, J. N. *Intermolecular and Surface Forces: with Applications to Colloidal and Biological Systems*; Academic Press: London, 1985; pp 249−257.
60. Hostetler, M. J.; Wingate, J. E.; Zhong, C. J.; Harris, J. E.; Vachet, R. W.; Clark, M. R.; Londono, J. D.; Green, S. J.; Stokes, J. J.; Wignall, G. D.; *et al.* Alkanethiolate Gold Cluster Molecules with Core Diameters from 1.5 to 5.2 nm: Core and Monolayer Properties as a Function of Core Size. *Langmuir* **1998,** *14*, 17–30.
61. Alvarez, M. M.; Khoury, J. T.; Schaaff, T. G.; Shafigullin, M. N.; Vezmar, I.; Whetten, R. L. Optical Absorption Spectra of Nanocrystal Gold Molecules. *J. Phys. Chem. B* **1997,** *101*, 3706–3712.
62. Schaaff, T. G.; Shafigullin, M. N.; Khoury, J. T.; Vezmar, I.; Whetten, R. L.; Cullen, W. G.; First, P. N.; GutierrezWing, C.; Ascensio, J.; JoseYacaman, M. J. Isolation of Smaller Nanocrystal Au Molecules: Robust Quantum Effects in Optical Spectra. *J. Phys. Chem. B* **1997,** *101*, 7885–7891.
63. Jin, R.; Egusa, S.; Scherer, N. F. Thermally-Induced Formation of Atomic Au Clusters and Conversion into Nanocubes. *J. Am. Chem. Soc.* **2004,** *126*, 9900–9901.
64. Zheng, J.; Zhang, C.; Dickson, R. M. Highly Fluorescent, Water-Soluble, Size-Tunable Gold Quantum Dots. *Phys. Rev. Lett.* **2004,** *93*, 077402.
65. Daniel, M. C.; Astruc, D. Gold nanoparticles: Assembly, Supramolecular Chemistry, Quantum-Size-Related Properties, and Applications toward Biology, Catalysis, and Nanotechnology. *Chem. Rev.* **2004,** *104*, 293–346.
66. Negishi, Y.; Tsukuda, T. One-Pot Preparation of Subnanometer-Sized Gold Clusters *via* Reduction and Stabilization by *meso*-2,3-Dimercaptosuccinic Acid. *J. Am. Chem. Soc.* **2003,** *125*, 4046–4047.
67. Luminescent materials were also obtained, which formed suspensions in water or methanol.
68. Longenberger, L.; Mills, G. Formation of Metal Particles in Aqueous-Solutions by Reactions of Metal-Complexes with Polymers. *J. Phys. Chem.* **1995,** *99*, 475–478.
69. Esumi, K.; Hosoya, T.; Suzuki, A.; Torigoe, K. Spontaneous Formation of Gold Nanoparticles in Aqueous Solution of Sugar-Persubstituted Poly(amidoamine) Dendrimers. *Langmuir* **2000,** *16*, 2978–2980.
70. Sakai, T.; Alexandridis, P. Mechanism of Gold Metal Ion Reduction, Nanoparticle Growth and Size Control in

Aqueous Amphiphilic Block Copolymer Solutions at Ambient Conditions. *J. Phys. Chem. B* **2005,** *109*, 7766–7777.
71. Sakai, T.; Alexandridis, P. Single-Step Synthesis and Stabilization of Metal Nanoparticles in Aqueous Pluronic Block Copolymer Solutions at Ambient Temperature. *Langmuir* **2004,** *20*, 8426–8430.
72. Boisselier, E.; Diallo, A. K.; Salmon, L.; Ornelas, C.; Ruiz, J.; Astruc, D. Encapsulation and Stabilization of Gold Nanoparticles with "Click" Polyethyleneglycol Dendrimers. *J. Am. Chem. Soc.* **2010,** *132*, 2729–2742.
73. Hoppe, C. E.; Lazzari, M.; Pardinas-Blanco, I.; Lopez-Quintela, M. A. One-Step Synthesis of Gold and Silver Hydrosols Using Poly(*N*-vinyl-2-pyrrolidone) as a Reducing Agent. *Langmuir* **2006,** *22*, 7027–7034.
74. Khullar, P.; Mahal, A.; Singh, V.; Banipal, T. S.; Kaur, G.; Bakshi, M. S. How PEO-PPO-PEO Triblock Polymer Micelles Control the Synthesis of Gold Nanoparticles: Temperature and Hydrophobic Effects. *Langmuir* **2010,** *26*, 11363–11371.
75. Brust, M.; Fink, J.; Bethell, D.; Schiffrin, D. J.; Kiely, C. Synthesis and Reactions of Functionalized Gold Nanoparticles. *J. Chem. Soc., Chem. Commun.* **1995,** 1655–1656.